A Novel Deep-learning Based Surrogate Modeling of Stochastic Electric Vehicle Traffic User Equilibrium in Low-Carbon Electricity-Transportation Nexus

Quan Yuan[a], Yujian Ye[a,*], Yi Tang[a], Yuanchang Liu[b] and Goran Strbac[c]

[a]School of Electrical Engineering, Southeast University, Sipailou 2, Nanjing, 210096, China
[b]Department of Mechanical Engineering, University College London, London, WC1E 7JE, UK
[c]Department of Electrical and Electronic Engineering, Imperial College London, London, SW7 2AZ, UK

ARTICLE INFO

Keywords:
Deep belief network
electric vehicle
edge-conditioned convolutional network
transportation electrification
traffic assignment problem
traffic user equilibrium

ABSTRACT

The increasing penetration of electric vehicles (EV) and fast charging stations (FCS) is tightly coupling the operation of power and transportation systems. In this context, the characterization of the EV flows and charging demand in response to varying traffic conditions and coordinated optimization strategies play a vital role. Previous work on the computation of stochastic traffic user equilibrium (TUE) involve non-linearities in the traffic link and FCS congestion representations and are generally inefficient in dealing with the multi-source uncertainties associated with the operating conditions of the traffic network (TN) and power distribution network (PDN). To address this, this paper proposed a novel deep learning (DL) based surrogate modeling method, leveraging the strength of edge-conditioned convolutional network (ECCN) and deep belief network (DBN). ECCN enables automatic extraction of spatial dependencies, taking into account both node and edge features characterizing the operation of TN. DBN leverages the value of the extracted features and achieves an accurate mapping between the latter to the EV charging demand and EV flows in the TUE, while adaptively generalizing to the multi-dimensional uncertainties. Case studies on three test systems of different scales (including a real-world case involving the matched TN and PDN of Nanjing city) demonstrate that the proposed surrogate model achieves a higher solution accuracy with respect to the state-of-the-art DL-based methods, and exhibits favourable computational performance. Quantitative results also corroborate the benefits brought by the proposed coordinated spatial optimization of EV flows and charging demand on the operation of both TN and PDN.

Nomenclature

A. Indices and Sets

$j \in J$	Index and set of O-D pairs.
$i \in I$	Index and set of paths.
$a \in A$	Index and set of transportation network (TN) links.
$z \in Z$	Index and set of fast charging stations (FCS).
$x, y \in X$	Index and Set of power distribution network (PDN) nodes.
$l \in L$	Index and Set of PDN lines.
$X^C \subset X$	Subset of PDN nodes with carbon capture storage (CCS).
X_x	Set of PDN nodes which connect to node x.

B. Parameters

λ_z	Locational electricity price at FCS z.
$\delta_{i,j,a}, \pi_{i,j,z}$	Binary indicators of whether link a or FCS z is in path i of O-D pair j or not.
c_a, c_z	Capacity of link a and FCS z.
t_a^0	Free traveling time of EV flows on link a.
t_z^0	Average charging time of EV flows at FCS z.
d_j	EV traveling demand of O-D pair j.
a_x, b_x	Quadratic and linear cost coefficients of distributed generator (DG) at node x.
r_{xy}^l, x_{xy}^l	Resistance and reactance of line l.
z_{xy}^l	Impedance of line l.
$\overline{I}^l$	Maximum current limit of line l.
$\underline{U}, \overline{U}$	Minimum and maximum voltage limits.
$\underline{P}_x^G, \overline{P}_x^G$	Minimum and maximum active power limits of DG at node x.
$\underline{Q}_x^G, \overline{Q}_x^G$	Minimum and maximum reactive power limits of DG at node x.
P_x^D, Q_x^D	Real and reactive power demand at node x.
β	Carbon emission intensity.
ϵ	Carbon capture efficiency.

C. Variables

$f_{i,j}$	EV flow on path i of O-D pair j.

*This work was supported by the 2021 Jiangsu Shuangchuang (Mass Innovation and Entrepreneurship) Talent Program (No. JSSCBS20210137).

*Corresponding author
yuanquan_seu@seu.edu.cn (Q. Yuan); yeyujian@seu.edu.cn (Y. Ye); tangyi@seu.edu.cn (Y. Tang); yuanchang.liu@ucl.ac.uk (Y. Liu); g.strbac@imperial.ac.uk (G. Strbac)
ORCID(s): 0000-0001-5028-4839 (Q. Yuan); 0000-0002-9278-9218 (Y. Ye); 0000-0002-2250-6024 (Y. Tang); 0000-0001-9306-297X (Y. Liu); 0000-0001-7421-3947 (G. Strbac)

s_a, s_z	EV flow on link a and at FCS z.
t_a	EV traveling time on link a.
t_z	EV charging waiting time at FCS z.
P_x^G, Q_x^G	Active and reactive power output of DG at node x.
P_x^C	Active power consumed by CCS at node x.
CE_x, CC_x	Carbon emission/captured by CCS at node x.
P_z^{EV}	Charging demand of EVs at FCS z.
P_{xy}^l, Q_{xy}^l	Active and reactive power flows on line l.
i_{xy}^l	Squared current magnitude on line l.
U_x	Squared voltage magnitude at node x.

1. Introduction

Environmental and economic concerns have paved the way for the deep decarbonization of energy systems through large-scale integration of renewable generation and transportation electrification, in China and beyond [1]. However, this paradigm shift introduces significant challenges to the operation and development of future power systems. At the generation side, the proliferation of uncertain and intermittent renewable generation challenges the system balancing. At the demand side, since transportation sector accounts for almost one third of the global energy demand, and more than 20% carbon footprint, its electrification has become an inevitable trend. However, the latter not only intensifies the overall electrical energy consumption, but also disproportionately increases the demand peaks, driven by the temporal patterns of users' driving requirement. Large-scale integration of electric vehicles (EV) and fast charging stations (FCS), coupes more seamlessly the operation of the transportation network (TN) and power distribution network (PDN) [2]. Latest statistics report that over 3.3 million FCS were built by 2020, and the EV stock is projected to expand from 4.92 million in 2020 to almost 50 million by 2030, with an annual growth of nearly 30% in China [3].

In this setting, the charging options for EVs generally include fast and slow charging. In the former, EVs are charged at home or workplace while they park for a long period of time. In this case, EVs are generally recognized as a representative type of shiftable loads that can participate in different demand response programs, and contribute to filling the gap between peak and valley demands, as well as offering auxiliary services to the upstream electricity system [4, 5]. Although these previous studies contribute to the optimal temporal management of EV charging loads in the PDN, the influence of the traffic condition on the EV navigation and subsequently its charging behaviors is neglected. The latter charging option is characterized by higher range anxiety and thus higher charging power, where EVs charge at the FCS built along the roads in TN. This option is primarily linked to the travel plan or the commuting behavior of EV users and thus the spatial distribution of EV charging loads. In this case, the optimization of EV charging demand necessitates to account for influencing factors in the TN such as traffic congestion, EV users' traveling demand as well as factors in the PDN, predominately the (locational) electricity prices which signal financial incentives for EV users [6, 7].

Previous works on the EV charging demand modeling considering fast charging can be broadly divided into two categories. The first category evaluates the charging demand from the perspective of a single EV driver. Given its origin-destination (O-D) pair, departure time, and specific traffic condition, an optimization problem is solved to select the optimal path corresponds to minimum driving distance or traveling time [8, 9, 10, 11]. However, self-interested behaviours of EV users may aggravate the traffic congestion and charging congestion (high queuing time) [12]. Conversely, the second category aims at determining the steady-state distribution of traffic flows, which is known as the *traffic assignment problem* (TAP). It considers congestions in traffic links and nodes caused by the aggregated movement of EVs and the selfish behavior of individual EV in route selection from the perspective of the transportation system. Striving at competing against each other for available road resources, the solution of the TAP is called an *traffic user equilibrium* (TUE) [13, 14, 15, 16], which signifies a condition that no EV owner can reduce its cost by changing the route or charging plan unilaterally.

However, the convectional solution procedure of the TAP faces the following challenges. First of all, in order to account for the congestion effect, the traveling time is commonly modeled as a *latency function* (such as the most widely used *Bureau of Public Roads* (BPR) function) of EV flows. This, however, introduces non-linearities in the TAP [7, 14, 16, 17], for which off-the-shelf solvers are available to guarantee convergence or global optimality. Furthermore, although authors in [17, 18, 19, 20], extend the deterministic TAP model to include random components in the travel cost functions to account for variations in the travelers' perception of travel cost and routing preferences presuming probability distributions. However, the examined TAP does not consider EV users' participation and thus the waiting time cost at the FCS and the cost of purchasing electrical energy from the PDN (and the involved uncertainties) are not considered in the objective of the TAP. Furthermore, it poses significant challenges to identify appropriate probability distributions and obtain a set of representative scenarios that captures all significant realizations of the multi-dimensional uncertainties involved in the TAP [21]. In view of the aforementioned computational challenges, alternative approaches need to be devised to address stochastic TAP with sufficient accuracy and efficiency.

Driven by the rapid advancements in artificial intelligence, deep learning (DL) has attracted increasing research interest in the industry and academic community and has emerged as a promising alternative to their model-based counterparts in solving large-scale optimization problems [22, 23, 24, 25, 26]. In a model-free way, DL methods facilitate to automatic feature extractions from provided

datasets and accurate model regression. Well-trained DL models exhibit high generalization capabilities which can be directly applied to new cases without costly numerical computation. Driven by these desirable properties, previous work has witnessed a increasing application of various DL methods in various challenging problems in power systems [27] and beyond.

Aims at addressing the limitations of previous approaches, this paper proposes a novel DL-based surrogate model for the stochastic TAP, combining the strength of *graph convolutional network* (GCN) and *deep belief network* (DBN). The novel contribution of this paper can be outlined as follows:

- Since the transportation system is intrinsically embedded with graph structure and the convolution layer has been the primary means of modeling spatial dependencies, an enhanced version of the GCN, namely the *edge conditioned convolutional* (ECCN) is adopted to extract features on spatial dependencies from raw graph data of the TN described by both edge and node features.

- Although previous work have employed GCN for forecasting the spatial distribution of traffic flows [28], the forecasted outcome fail to describe the steady-state distribution of EV flows as expressed in the TUE, since the regression task is carried out without taking inputs from the TAP. To this end, we leveraged the value of the extracted features and construct a surrogate model to map them to the EV charging demand and EV flows in the TUE.

- Previous study [29] demonstrated that when the network architecture gets deeper, it becomes more challenging to obtain good generalization performance using *deep neural networks* (DNN). However, much better results could be achieved using DBN when each layer is pre-trained [30]. Driven by this property, DBN is employed to construct a surrogate model to map the extracted features to the optimal EV charging demand and EV flows in the TUE solution. Empowered by the excellent generalization capability of DBN, the surrogate model copes well with the multi-dimensional uncertainties in the TAP.

- Case studies on an 6-node system, 24-node system, and a real-world 124-node system of Nanjing city comprehensively highlight the superior performance of the proposed surrogate modeling approach by comparing it against the state-of-the-art DL-based supervised learning approaches. Results also confirm the benefits brought by the proposed spatial optimization of EV flows and charging demand on the operation of the TN and PDN.

The rest of this paper is organized as follows. Section 2 provides the detailed mathematical formulation of TAP-TUE. Section 3 details the proposed DL-based surrogate modeling framework of the EV TUE, orchestrating the working principals of ECCN and DBN. Section 4 outlines the optimal operation model of a low-carbon PDN considering the participation of renewable generation, EV and carbon capture storage. Section 5 carries out comprehensive case studies to validate the effectiveness of the proposed method. Finally, Section 6 discusses conclusions of this work.

2. Formulation of EV Traffic Assignment Problem-Traffic User Equilibrium

The TN can be abstractly described by a connected graph $G = [N, A]$. Each EV traveling in G departs from an origin O and arrives at a destination D. A path is composed of multiple end-to-end connected links, while a link can be shared by multiple different paths. Each O-D pair can be connected by different paths, where the EV flows will be distributed to.

The TAP-TUE problem can be formulated as follows:

$$\min \sum_{a\in A}\omega\int_0^{s_a} t_a(\mathrm{n})\mathrm{dn}+\sum_{z\in Z}\left(\omega\int_0^{s_z} t_z(\mathrm{n})\mathrm{dn}+\lambda_z P_z t_z^0 s_z\right) \quad (1)$$

subject to:

$$s_a = \sum_{j\in J}\sum_{i\in I_j} f_{i,j}\delta_{i,j,a}, \forall a \quad (2)$$

$$s_z = \sum_{j\in J}\sum_{i\in I_j} f_{i,j}\pi_{i,j,z}, \forall z \quad (3)$$

$$t_a(s_a) = t_a^0\left(1+0.15(s_a/c_a)^4\right), \forall a \quad (4)$$

$$t_z(s_z) = t_z^0\left(1+\mu s_z/(c_z-s_z)\right), \forall z \quad (5)$$

$$f_{i,j} \geq 0, \forall i, \forall j \quad (6)$$

$$\sum_{i\in I_j} f_{i,j} = d_j, \forall j \quad (7)$$

$$P_z^{EV} = \sum_{j\in J}\sum_{i\in I_j} f_{i,j}\pi_{i,j,z}P_z, \forall z \quad (8)$$

The objective function (1) is composed of three cost components: i) total travel time cost on the links, ii) total waiting time cost at FCS, and iii) total electricity purchasing cost from PDN at FCS. ω denotes the value of time. Constraints (2) and (3) describe the relationships between the path flow $f_{i,j}$ and flows on link a and at FCS z. Driven by the congestion effect, the traveling time of EVs on link a is represented as an BPR latency function of the EV flows, following the commonly adopted practice in [14, 15, 16]. Essentially, constraint (4) suggests that the flow on link a is not strictly bounded by its capacity c_a, congestion will be penalized through a sharp increase in the traveling time. The *Davidson function* [16] based on the *queuing theory* is employed to model the queuing time of EV flows at FCS z, as expressed in constraint (5). Constraints (6) and (7) ensure that all path flows are non-negative, and the summation of flows over all connecting paths for an O-D pair j equals to the EV traveling demand of the same O-D pair. Constraint (8) bridges the connection between the EV charging demand at FCS z and EV flow $f_{i,j}$.

The sources of nonlinearities in the TAP-TUE formulation include the nonlinear BPR latency function and Davidson function. These nonlinear functions can be approximated by piece-wise linear (PWL) functions and integrated

in TAP-TUE problem as linear constraints with integer variables, such as the method in [31]. In this paper, the PWL approximation is performed by introducing *type 2 special ordered set variables* (SOS2), which promises more efficient branching strategies, and is desirable for branch-and-bound solvers [32]. To perform SOS2 linearization on constraint (4) for example, we partition the feasible interval of s_a is into smaller segments. In each segment, $t_a(s_a)$ is approximated by a linear function, and constraint (4) can be re-expressed as:

$$\begin{aligned} s_a = \sum_m s_a^m \eta_a^m, t_a = \sum_m t_a(s_a^m)\eta_a^m, \forall a \\ \sum_m \eta_a^m = 1, 0 \le \{\eta_a^m, \forall m\} \in \text{SOS2}, \forall a \end{aligned} \tag{9}$$

where s_a^m denotes the break point of each segment, and η_a^m denotes continuous weights of each segment. The SOS2 linearization of (5) can be carried out in the same logic.

It can be observed from the formulation of TAP-UE problem that the source of stochasticity comprises the ones associated with the FCS nodes of the TN, including parameters λ_z, P_z, c_z, t_z^0, the ones associated with the links of the TN, including parameters t_a^0 and c_a, as well as parameter d_j which is associated with the O-D pairs. It is constructive to highlight that previous works [14, 17] largely focused only on the stochastic O-D demand while they neglect the ones associated with the operation status of the TN links and FCS. As discussed in Section I, in view of such multi-dimensional uncertainties, it is not possible to accurately characterize such uncertainties using probabilistic modeling approaches and in addition, the computational performance of model-based optimization method deteriorates when the scale of the problem increases. To purse higher generalization performance and higher computational efficiency at the same time, we propose a novel DL-based methodological framework to tackle this challenging problem.

3. Proposed DL-based Surrogate Modeling of EV Traffic User Equilibrium

To properly derive an effective data-driven DL-based modeling framework to replace the process of repeated solving TAP-TUE for different uncertain scenarios, we identify the following two main objectives to achieve. First, it necessitates excellent data perception capabilities in order to characterize the spatial dependencies of the high-dimensional uncertainties. Upon extracting these meaningful features, it then calls for a suitable model which can accurately map the former to the EV charging demand with excellent generalization capability. In the following subsections, we propose tailor-designed DL-based techniques to achieve these two objectives.

3.1. Edge Conditioned Convolution Network

Perception and interpreting raw TN features/parameters in terms of real-world spatial dependencies is challenging. A growing effort therefore has been witnessed in recent years in forecasting EV distribution with extraction of spatial features. In [33, 34], the convolutional neural networks (CNN) are employed to extract spatial dependencies. Although CNNs promise benefits for extracting spatial relationships in the *Euclidean space* as represented by two-dimensional images, they are inherently ineffective in dealing with the topological structure and the physical attributes of the TN. To this end, the convolution operators have been extended to *noneuclidean data* using graph convolutional networks (GCN) [28].

GCN utilizes the adjacency matrix to depict the structure of a graph. Provided an adjacency matrix $\boldsymbol{A}$, GCN constructs a filter in the Fourier domain. The filter, acting on the nodes of a graph, captures the spatial features between the nodes by its first-order neighborhood, then GCN is formed by stacking multiple convolutional layers, as expressed by:

$$\boldsymbol{H^{(l+1)}} = \sigma(\hat{\boldsymbol{D}}^{-\frac{1}{2}}\hat{\boldsymbol{A}}\hat{\boldsymbol{D}}^{-\frac{1}{2}}\boldsymbol{H^{(l)}}\boldsymbol{\theta^{(l)}}) \tag{10}$$

where $\boldsymbol{H^{(l)}}$ constitutes the feature matrix in layer l; the trainable weight matrix of layer l is denoted by $\boldsymbol{\theta^{(l)}}$, representing a linear transformation to map the feature space; $\sigma(\cdot)$ represents the sigmoid activation function; $\hat{\boldsymbol{A}} = \boldsymbol{A} + \boldsymbol{I}$ denotes the adjacent matrix with a self-loop connection, $\hat{\boldsymbol{D}}$ is the diagonal degree matrix (the number of edges terminating at each node) which aims to normalize $\boldsymbol{D}$ for re-scaling the aggregated information of a specific node from its neighbors.

It can be observed that the graph convolution operation requires only the input of the node features from the previous layer, and therefore cannot capture the impact of the edge features of the previous layer in the extracted spatial dependencies. To address this, the *edge conditioned filters* [35] are employed. Let $\boldsymbol{F_N}$ and $\boldsymbol{F_A}$ represent the node and edge feature matrix, respectively. At the input layer, $\boldsymbol{F_N^{(0)}}$ encapsulates the raw node features comprising the EV charging power P_z, average charging time t_z^0, locational electricity price signals λ_z, and the capacity c_z defined at each FCS z of the TN; while $\boldsymbol{F_A^{(0)}}$ describes the raw edge features comprising the free traveling time t_a^0 and capacity c_a of each link a. Note that the dimension of the node feature varies with the layer index, while the dimension of the edge feature stays constant. Let us define neighborhood $B(n) = \{m; (m,n) \in \boldsymbol{A}\} \cup \{n\}$ of node n to contain all adjacent nodes (predecessors in directed graphs) including n itself (self-loop).

The structure of ECCN is illustrated in Fig. 1, the node features $\boldsymbol{F_N^{(l)}}(n)$ at node n is defined as a weighted sum of features $\boldsymbol{F_N^{(l-1)}}(n)$ in its neighborhood $m \in B(n)$. The edge-conditioned convolution operation can be expressed as:

$$\boldsymbol{F_N^{(l)}}(n) = \frac{1}{|B(n)|}\sum_{m\in B(n)} \boldsymbol{\Theta_{mn}^{(l)}}\boldsymbol{F_N^{(l-1)}}(m) + \boldsymbol{b^{(l)}} \tag{11}$$

where $\boldsymbol{\Theta_{mn}^{(l)}}$ and $\boldsymbol{b^{(l)}}$ are trainable weights and bias.

As such, it can be observed that both node and edge features are utilized by the ECCN to extract the spatial dependencies, resulting in better perception of the multi-dimensional uncertainties of the TN.

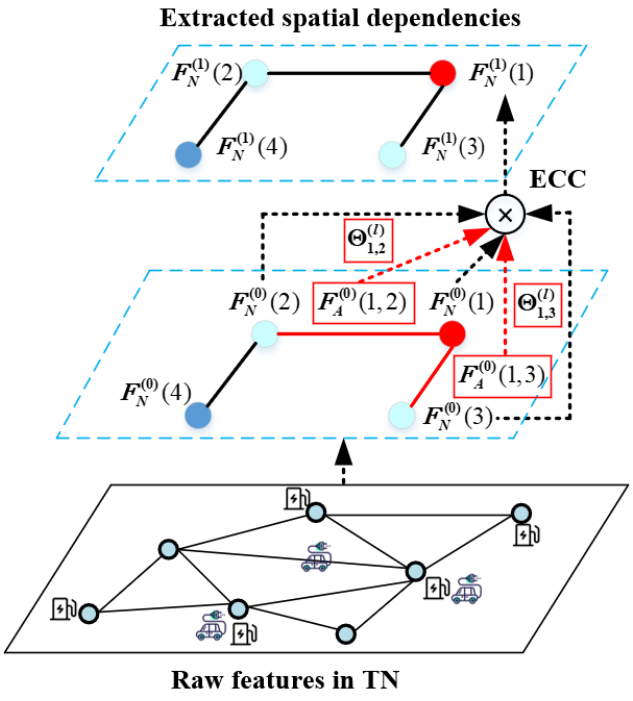

Figure 1: Schematic representation of ECCN-based spatial dependencies extraction.

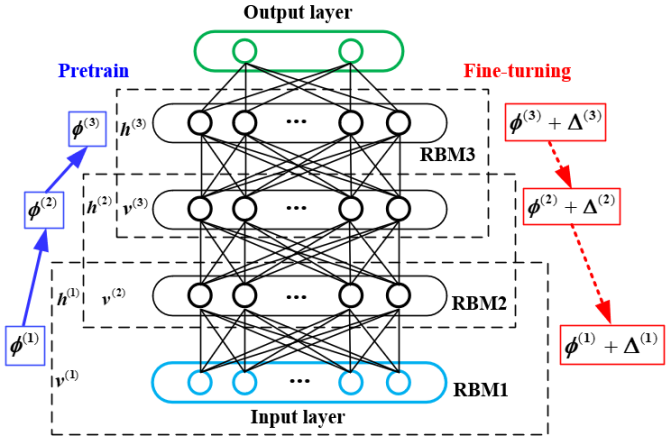

Figure 2: Structure of DBN-based regression model.

3.2. Deep Belief Network

Despite previous effort in applying GCN for spatial traffic flows forecasting [28], the regression process does not reflect the individual rationalities of EV owners and thus fail to characterize a stable traffic flow pattern in a congested TN. To this end, and having established excellent perception capability empowered by ECCN of the multi-dimensional uncertainties of the TN, a novel surrogate modeling method based on deep belief network (DBN) is proposed to map the extracted spatial features to the optimal EV charging demand at each FCS and the EV flow at each link in the TUE.

DBNs are generally characterized as probabilistic generative models constructed by stacking up *Restricted Boltzmann Machines* (RBMs) [30] (Fig. 2). DBN has received huge success in power system forecasting applications [27], such as short-term load [36], wind [37], and PV [38]. In this paper, we leverage its performance to forecast the optimal solution of the TUE problem based on the extracted discriminative features from the ECCN.

The training of DBN is illustrated in Fig. 2, which comprises the following two steps:

Step 1: This step involves a *layer-wise pre-training* procedure for each RBM, which consists of a visible layer and a hidden layer. The first RBM is trained by feeding in the data (in our case the extracted features from ECCN, $\boldsymbol{v}^{(1)}$) and fixing the parameters of this RBM. As the network gets deeper, the relationship between the RBM input and hidden layers can be defined as an energy function:

$$E^{(l)}(\boldsymbol{v},\boldsymbol{h}|\boldsymbol{\phi}^{(l)}) = -(\boldsymbol{a}^{\mathrm{T}}\boldsymbol{v} + \boldsymbol{b}^{\mathrm{T}}\boldsymbol{h} + \boldsymbol{v}^{\mathrm{T}}\boldsymbol{w}\boldsymbol{h}) \tag{12}$$

where $\boldsymbol{v}$ and $\boldsymbol{h}$ denote the visible units and hidden units for layer l, respectively. $\boldsymbol{a}$ and $\boldsymbol{b}$ denote the bias of the visible and hidden units, and $\boldsymbol{w}$ denotes the weights of the connection between the visible and hidden units, and $\boldsymbol{\phi}^{(l)} = [a_v, b_h, w_{vh}]$ denotes the collection of all trainable weights of RBM l.

The joint probability distribution over $\boldsymbol{v}$ and $\boldsymbol{h}$ can be defined as:

$$P^{(l)}(\boldsymbol{v},\boldsymbol{h}|\boldsymbol{\phi}^{(l)}) = \frac{1}{Z(\boldsymbol{\phi}^{(l)})}\mathrm{e}^{-E^{(l)}(\boldsymbol{v},\boldsymbol{h}|\boldsymbol{\phi}^{(l)})} \tag{13}$$

where $Z(\boldsymbol{\phi}^{(l)}) = \sum_{\boldsymbol{v}}\sum_{\boldsymbol{h}}\mathrm{e}^{E^{(l)}(\boldsymbol{v},\boldsymbol{h}|\boldsymbol{\phi}^{(l)})}$ is a normalization factor to purse unity probability.

Connections between RBMs are bi-directional and symmetric, which suggests that both directions share the common weights (i.e. $\boldsymbol{h}^{(l)} = \boldsymbol{v}^{(l+1)}$) and information flows in both directions. In order to ensure that the feature information is retained when it is mapped to different feature spaces, each RBM needs to be trained separately. Given the learning sample set $\boldsymbol{S}$, the task of pre-training RBM is to identify suitable weights $\boldsymbol{\phi}$ which maximize the probability likelihood function of $\boldsymbol{S}$, the corresponding loss function can be expressed as:

$$\min\ L(\boldsymbol{\phi},\boldsymbol{S}) = -\sum_{\boldsymbol{v}\in\boldsymbol{S}}\log\sum_{\boldsymbol{h}}\frac{\mathrm{e}^{E(\boldsymbol{v},\boldsymbol{h}|\boldsymbol{\phi})}}{Z(\boldsymbol{\phi})} \tag{14}$$

By pre-training each RBM, the connection relation between each RBM can be learned without any label information, through a unsupervised learning algorithm [39].

Step 2: This step involves a *fine-turning* process. The back-propagation (BP) algorithm is employed to adjust the weights of the pre-trained model for further performance improvement. The output layer of the DBN produces the EV charging demand and EV flow, and the loss function is the mean square error (MSE) between the forecasted output and the label generated by solving the TAP-TUE problem.

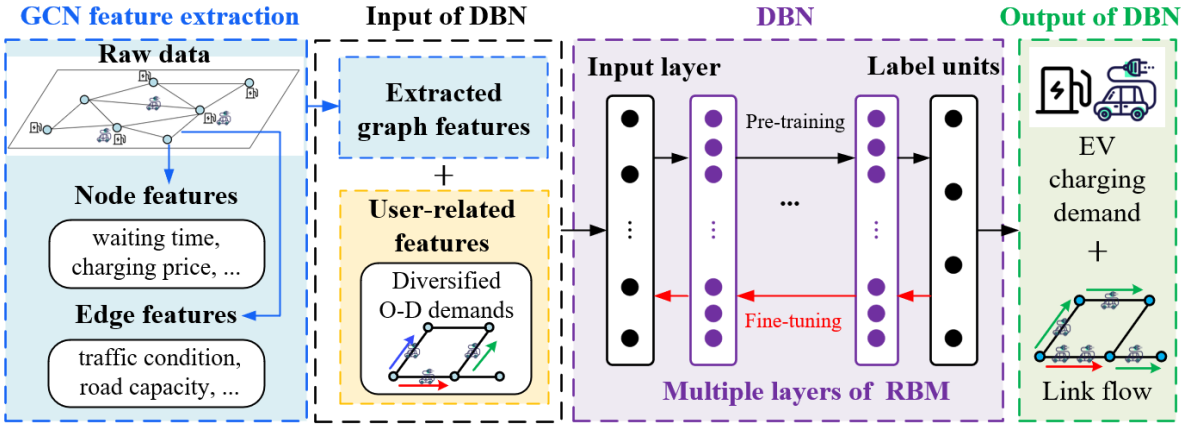

Figure 3: Structure of the proposed surrogate model.

$$\text{MSE} = \frac{1}{NM}\sum_{n=1}^{N}\sum_{m=1}^{M}(\boldsymbol{y}_n(m) - \boldsymbol{y}_n^*(m))^2 \tag{15}$$

where N is the number of test output samples, and M is the dimension of output. $\boldsymbol{y}_n(m)$ and $\boldsymbol{y}_n^*(m)$ are respectively the real output and forecasted output for m-th output of the n-th sample.

The BP process adjusts the parameters of DBN, and finally the parameters $\boldsymbol{W}^{(l)} = \boldsymbol{\phi}^{(l)} + \boldsymbol{\Delta}^{(l)}, \forall l$ of DBN are obtained, where $\boldsymbol{\Delta}^{(l)}$ represents the amount of learned fine-tuning on weights of layer l based on the label information.

The overall framework of the proposed DL-based surrogate model is illustrated in Fig. 3.

4. Modeling Low-Carbon Power Distribution Network with EV Charging Demand

The FCS of TN are served by a PDN, which is usually a radial network, and can be represented by a tree topology. Having established a generalizable mapping between the TN uncertainties to the EV charging demand through the surrogate model, the PDN is modeled by the alternating current optimal power flow (ACOPF). Since this problem is non-convex and NP-hard, to pursue computational tractability, convex relaxation is performed, which transfers the ACOPF problem to a *second order conic program* (SOCP) [15]. In addition to the beneficial impact promised by mobile flexible resources such as EVs (such as directing EV flows to FCS connected by abundant wind resources) in decarbonization of the distribution system, we further explore the beneficial impact from non-mobile resources such as carbon capture storage (CCS) in reducing carbon emissions of co-located distributed generators (DG) [40]. The modified SOCP considering the integration of DG, photovoltaics (PV), EV and CCS can be formulated as:

$$\min \sum_{x}\left(a_x(P_x^G)^2 + b_x P_x^G\right) \tag{16}$$

subject to:

$$P_{xy}^l + P_y^{NG} - r_{xy}^l i_{xy}^l = \sum_{r\in X_y} P_{yr}^l + P_y^D, \forall l \tag{17}$$

$$Q_{xy}^l + Q_y^G - x_{xy}^l i_{xy}^l = \sum_{r\in X_y} Q_{yr}^l + Q_y^D, \forall l \tag{18}$$

$$U_y = U_x - 2(r_{xy}^l P_{xy}^l + x_{xy}^l Q_{xy}^l) + (z_{xy}^l)^2 i_{xy}^l, \forall l \tag{19}$$

$$i_{xy}^l U_x \geq (P_{xy}^l)^2 + (Q_{xy}^l)^2, \forall l \tag{20}$$

$$i_{xy}^l \leq (\overline{I}^l)^2, P_{xy}^l \geq 0, Q_{xy}^l \geq 0, \forall l \tag{21}$$

$$\underline{P}_x^G \leq P_x^G \leq \overline{P}_x^G, \underline{Q}_x^G \leq Q_x^G \leq \overline{Q}_x^G, \forall x \tag{22}$$

$$(\underline{U})^2 \leq U_x \leq (\overline{U})^2, \forall x \tag{23}$$

$$CE_x = \beta P_x^G - CC_x, \forall x \in X^C \tag{24}$$

$$CE_x = \beta P_x^G, \forall x \in X \setminus X^C \tag{25}$$

$$CC_x = \epsilon P_x^C, \forall x \in X^C \tag{26}$$

$$P_x^{NG} = P_x^G - P_x^C, \forall x \in X^C \tag{27}$$

The objective function (16) of the SOCP lies in minimizing the total generation costs in the PDN. Constraints (17)-(18) express the nodal active and reactive power balance for the PDN. Constraints (19)-(23) are associated with the SOCP relaxation for optimal power flow [15]. Constraints (24)-(25) represent the carbon emission for DGs with and without CCS, respectively. Constraints (26)-(27) represent the net power output of DGs with CCS, in which the latter consumes power generated by the DGs for carbon capture.

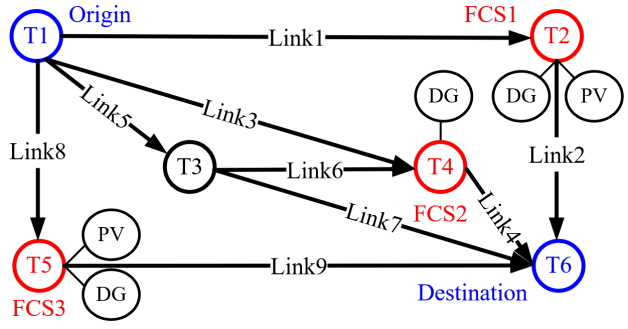

Figure 4: Topology of the 6-node test system.

Table 1
Mean μ, standard deviation σ and range R correspond to the truncated normal distributions of uncertain parameters

	λ_z(CNY/kWh)	t_a^0(h)	t_z^0(h)	P_z(kW)	d_j(veh)
μ	{0.75,1,0.75}	0.25	0.5	100	1000
σ	0.2	0.1	0.2	30	200
R	[0.5,1.5]	[0.1,0.4]	[0.1,1]	[50,200]	[800,1200]

5. Case Studies

5.1. Test case 1: 6-node System

The topology of the 6-node system with 9 traffic links is shown in Fig. 4. Three FCS with 600veh/h capacity and 100kW charging power are located at nodes 2, 3, and 4, unity power factor for EV charging demand is assumed. The parameter of Davidson function is set as $\mu = 0.05$. The O-D demand is set to 1,000veh/h from node 1 to node 6. The capacity of each link in TN is 400veh/h, and the value of unit time is set as $\omega = 30$CNY/h. Distribution lines are omitted in this small case for the sake of brevity. DGs are located at nodes 2, 4, and 5, while PV generators are located at nodes 2 and 5. DG share the same set of cost parameters: $a = 1{,}000\text{CNY/(kWh)}^2$ and $b = 65{,}000$CNY/kWh.

For the data generating process, we first simulate different scenarios to characterize the variation of the core influencing uncertain parameters in the TN (Section 2) including the locational electricity prices, free traveling time, average charging time, charging power, and the O-D travel demand. Their values are generated by sampling the respective truncated normal distributions with the mean, standard deviation, and range for each of the parameters shown in Table 1. Next, the linearized TAP-TUE problem is solved for each of these scenarios to generate the associated label, namely the EV charging demand and the EV flow in each link. A total of 1,000 samples are generated, of which 100 samples are employed for performance evaluation. To validate the effectiveness of the proposed surrogate modeling method (ECCN-DBN), we benchmark its performance against a number of DL-based methods including DNN, ECCN-DNN and DBN. Each of these methods is trained for 100 epochs, and their performance are assessed every 20 epochs during training by evaluating it on the test set.

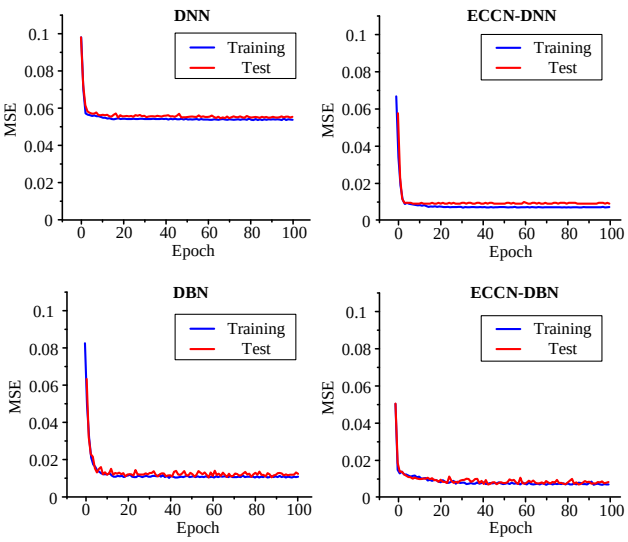

Figure 5: Training and test MSE for different DL-based methods.

Table 2
Training and test MSE at convergence and average TAP-TUE cost (in CNY) for different DL-based methods

Method	DNN	ECCN-DNN	DBN	ECCN-DBN
Training MSE	0.0550	0.0086	0.0105	0.0075
Test MSE	0.0570	0.0094	0.0113	0.0076
TAP-TUE cost	62,250	41,532	42,570	40,968

Fig. 5 illustrates the training and test MSE for the investigated four DL-based methods, and their values at convergence are presented in Table 2. Our first observation is that DBN outperforms DNN with regard to both the training and test MSE. The rationale behind this performance superiority lies in the pre-training process in the DBN training. A greedy learning algorithm is utilized to find a fairly good set of initial parameters quickly, and later the model's fitting ability can be enhanced through a supervised fine-tuning procedure. This proves to be particular beneficial in leveraging the generalization capability of the model with deeper network architectures [29]. As discussed in Section III-A, both node and edge features of the TN can be effectively utilized by the ECCN to extract the spatial dependencies. As such, it can be observed that ECCN contributes significantly to the reduction of both training and test losses. Overall, the proposed ECCN-DBN method exhibits the best performance. In relative terms, the proposed method achieves 86.67%, 19.15%, and 32.74% lower test MSE and 34.19%, 1.36%, and 3.76% lower average TAP-TUE cost (over the test set) compared to DNN, ECCN-DNN and DBN, respectively. This corroborates the high accuracy and excellent generalization capability of the proposed DL-based methods in uncertain scenarios of TN which are not encountered in the training process.

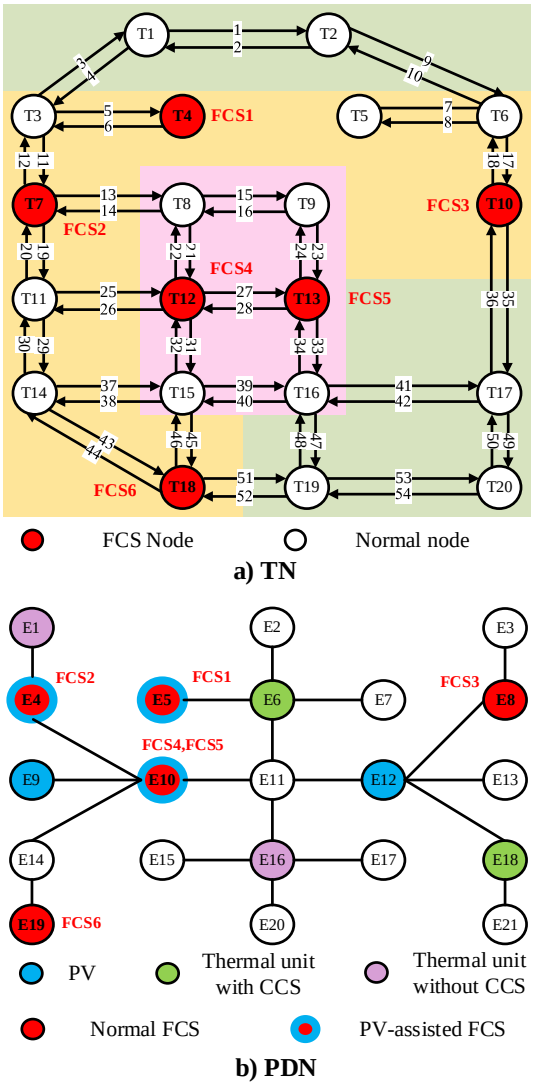

Figure 6: Topology of the coupled 20-node TN and 21-node PDN system.

5.2. Test case 2: 20-node TN and 21-node PDN System

Having established the superior performance of the proposed ECCN-DBN method, the aim of this subsection lies in uncovering the beneficial impact of the proposed coordinated optimization of EV charging demand against a uncoordinated case where all EV users select the shortest path between O-D and the FCS with lowest charging price employing the Dijkstra's algorithm [41].

The topology of the 20-node TN and 21-node PDN is shown in Fig. 6. The TN involves 54 traffic links and 6 FCS located at node T4, T7, T10, T12, T13, T18 (referred to as FCS 1-6), of which FCS 1, 2, 4 and 5 are characterized by PV-assisted stations. The connected location of FCS in the PDN is highlighted in Fig. 6(b) in red font next to the relevant PDN node. The charging power and capacity of each FCS are 100kW and 2,800veh/h, respectively, and the capacity of each link is 1,200 veh/h. The O-D demand is set to 10,000veh/h. In order to reflect the diversity of EV users in O-D choice, we partition the TN into three different regions highlighted with different colors in Fig. 6(a). Nodes at each region correspond to different probabilities to be sampled as an EV user's origin or destination. In this case, the probability corresponding to pink/yellow/green region is 0.6/0.25/0.15, resembling a case that the city center is the most popular choice for EV traveling demand. The parameters related to the SOCP implementation of the PDN, associated with DG, fixed demand, PV, CCS are organized in a dataset uploaded to an online database [42]. The locational prices are computed by solving the SOCP problem without considering the charging demand of EVs. Following a similar data generating process for test case 1, the computed prices are used as mean values to further generate scenarios of prices using a truncated normal distribution. The scenarios of the rest of the uncertain parameters in the TN is generated analogously. A total of 10,000 samples are generated and a 90%/10% train/test split ratio is adopted.

Table 3
Aggregate EV Charging demand (in MW) at each FCS under coordinated and uncoordinated scenarios

Aggregate EV charging demand	Uncoordinated	Coordinated
FCS 1	64.80	134.31
FCS 2	134.73	141.30
FCS 3	131.49	139.95
FCS 4	189.67	170.10
FCS 5	228.02	175.14
FCS 6	151.29	142.20

Let us first demonstrate the benefits of the proposed method associated with the operation of TN. Table 3 compares the aggregate EV charging demand at each FCS P_z^{EV} under the coordinated and uncoordinated scenarios. It can be observed that the EV charging demand mostly concentrate at FCS 4 and 5 in the uncoordinated scenario. As a result, the EV flow on link 14, 15, 16, 17, 21, 23, 24, 27, 28, 31, 33, 34 and 45 has exceeded the link capacity of 1,200veh/h, contributing to traffic congestions (Fig. 7). Furthermore, the charging waiting time at FCS 4 and 5 is significantly higher in the uncoordinated scenario with respect to the coordinated one, as depicted in Fig. 8. In contrast, traffic congestions are eliminated under the coordinated scenario where the aggregated EV charging demand is distributed more evenly across all FCS (Table 3) in the TN, and as a result, the charging waiting time adheres to the same trend. Driven by these benefits, the TAP-TUE cost in the coordinated scenario is reduced by 20.26% with respect to the uncoordinated scenario.

Let us next demonstrate the benefits of the proposed method associated with the operation of PDN. Fig. 9 highlights the thermal DG dispatch, PV absorption and carbon captured under uncoordinated (indicated in black font) and coordinated (indicated in red font) scenarios. Table 4 summarizes the relevant statistics associated with the operation of the PDN under these two scenarios.

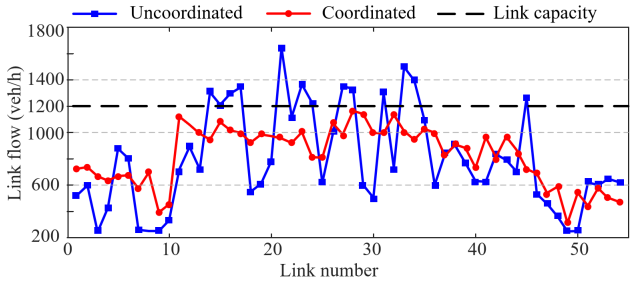

Figure 7: EV flow on each link under coordinated and uncoordinated scenarios.

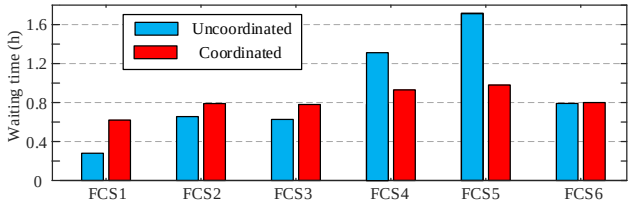

Figure 8: Charging waiting time at each FCS under coordinated and uncoordinated scenarios.

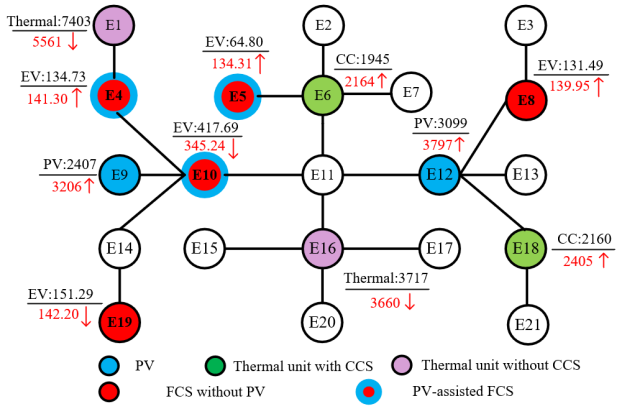

Figure 9: DG dispatch, PV absorption and carbon captured under uncoordinated and coordinated scenarios.

Table 4
Statistics associated with the operation of the PDN under uncoordinated and coordinated scenarios

Item	Uncoordinated	Coordinated
DG output (MW)	27,134	25,635
PV absorption (MW)	5,506	7,003
Generation cost (mil. CNY)	752	674
Net loss (MW)	565.2	378
Carbon capture (ton)	4,105	4,569
Carbon emission (ton)	19,202	17,733

According to Table 4, it can be determined that a more evenly distributed EV charging demand (Table 3) contributes to the reduction of the thermal DG outputs overall by 5.52%, the increase of PV absorption overall by 27.19%, by scheduling EV flows to PV-assisted FCS as well as to nodes close to PV generators. This leads to the reduction in the total generation cost and net loss of the PDN by 10.37% and 2.5%, respectively. The optimized spatial distribution of mobile EV resources, combined with the beneficial impact of CCS in capturing carbon emissions locally (an overall increase of 11.30% carbon captured is achieved), contributes to an overall reduction of 7.65% in carbon emission.

Table 5
Hyperparameters of ECCN and DBN in three test cases

Hyperparameter	Case 1	Case 2	Case 3
Dimension of ECCN input	33	134	896
Dimension of DBN output	15	74	524
Number of RBM layers	10	20	100
Number of RBM neurons	16	32	128
Learning rate	0.005	0.005	0.01
Batch size	16	64	256
Epoch	100	1,000	10,000
Optimizer		Adam	
Activation function		ReLU	

5.3. Test case 3: 124-node TN and 118-node PDN System of Nanjing City

In this section, we further validate the benefits of the proposed coordinated optimization method of EV flows and charging demand on a real-world case involving the 124-node TN and 118-node PDN System of Nanjing City [11]. Furthermore, we analyze the scalability of the proposed method considering different scales of the test systems (Sections 5.1-5.3).

The topology of this test system is depcited in Fig. 10. It should be highlighted that this paper is the first piece of work which showcases the performance of a coordination method of EV flows and charging demand on a real-world scale test system with a size of both TN and PDN far larger than the test systems involved in the previous studies. The examined TN involves 24 FCS, and the red lines refer to the links located at central area of Nanjing, a region of particular interest to our study. The charging power and capacity of each FCS are set as 100kW and 2,800veh/h, respectively, and the capacity of each link is 1,200 veh/h. The O-D demand is set to 30,000veh/h. In this case, the probability to be sampled as an EV user's origin or destination in the central and non-central region is set to 0.7 and 0.3, respectively, following a similar logic as in the test case 2 (Section 5.2). The parameters related to the SOCP implementation of the PDN are reward in the online datasheet [42]. Following a similar data generating process for test case 2, the computed prices are used as mean values to further generate scenarios of prices using a truncated normal distribution. The scenarios of the rest of the uncertain parameters in the TN is generated in a similar fashion. A total of 50,000 samples are generated and a 90%/10% train/test split ratio is adopted.

The hyperparameters of ECCN and DBN in the three test cases are listed as Table 5.

Fig. 11 depicts the spatial distribution of EV charging demand over the 24 FCS in the TN. A similar trend can be observed in the coordinated scenario that the EV charging demand is more smoothly distributed to FCS. This effect is

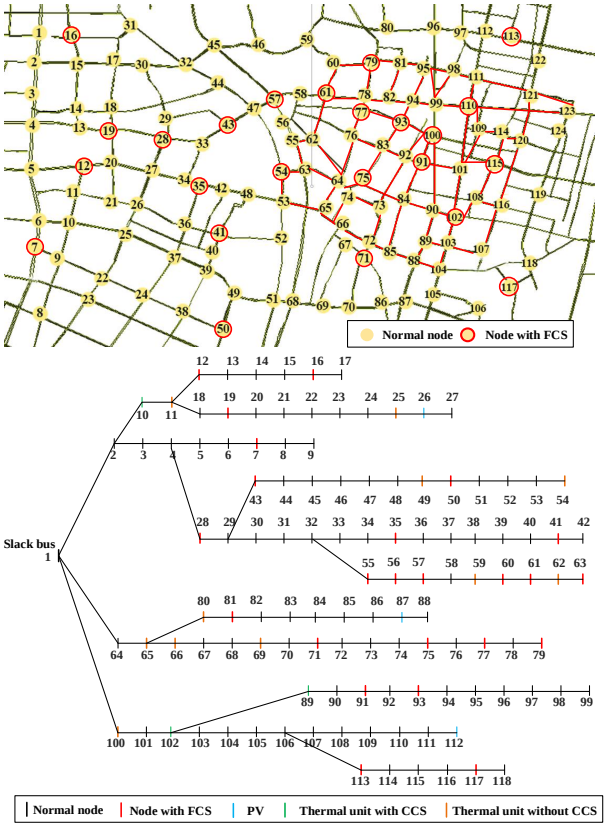

Figure 10: Topology of the 124-node TN and 118-node PDN system.

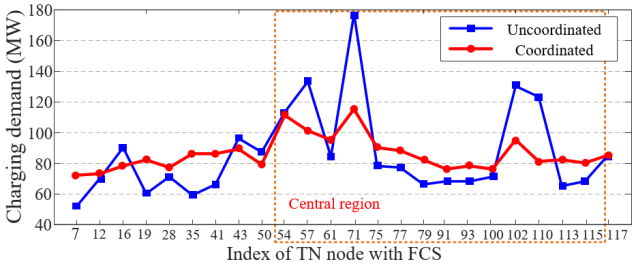

Figure 11: Aggregate EV Charging demand at each FCS under coordinated and uncoordinated scenarios.

prominent in the central region, which in turn, reduces the TAP-TUE cost in the coordinated scenario by 9.49% with respect to the uncoordinated scenario.

The associated benefits to the operation of the PDN are highlighted in Table 6. In relative terms, the DG output is reduced overall by 3.79% and the PV absorption is increased overall by 12.84%. This contributes to the reduction in the total generation cost and net loss of the PDN by 7.40% and 21.08%, respectively. The flexibility exploited from mobile and local CCS contributes to an overall reduction of 5.54% in carbon emission. The carbon captured increased by 11.36%.

Table 7 summarizes the results of the scalability analysis by presenting the solution quality (assessed through the percentage increase difference of TAP-TUE cost obtained

Table 6
Numerical results in PDN under coordinated and uncoordinated scenarios

Item	Uncoordinated	Coordinated
DG output (MW)	64,706	62,254
PV absorption (MW)	8,964	10,115
Generation cost (mil. CNY)	4,229	3,916
Net loss (MW)	1,570	1,239
Carbon capture (ton)	5,830	6,492
Carbon emission (ton)	50,464	47,669

Table 7
Scalability Analysis of proposed method considering different system scales.

Case	TN cost difference	Execution time (ms)
6 nodes	0.75%	37.89
20 nodes	0.92%	39.05
124 nodes	0.95%	44.31

by ECCN-DBN with respect to the theoretical optimum obtained by solving the model-based TAP-TUE optimization for all the test data samples) and the computational performance (assessed through the execution time) for each of the examined test cases (Sections 5.1-5.3).

It can be observed that the proposed surrogate method exhibits excellent generalization capability as the average achieved TAP-TUE cost is very close to the theoretical optimum regardless of the scale of the test systems. Furthermore, the proposed surrogate method also merits computational efficiency, since after off-line training, the execution time (i.e. the computational time to map a real-world TN and PND operation condition to the TUE EV flows and charging demand) of ECCN-DBN is always on timescales of milliseconds irrespective of the scale of the test systems.

6. Conclusions

In the context of harvesting the significant EV flexibility potential in electricity-transportation nexus, this paper has proposed a novel DL-based surrogate method to tackle the challenges of accurate and efficient identification of TUE in stochastic TAP. The proposed method combines the strength of the ECCN and DBN. ECCN, leveraging the performance of GCN, promises automatic feature extraction functionality, facilitating more accurate perception and interpretation of both node and edge features of TN in terms of their spatial dependencies; while DBN contributes to an accurate mapping of the extracted features to the EV charging demand and EV flows in the TUE. Case studies on three test systems of different scales (including a real-world test system of Nanjing city) have demonstrated the superior performance of the proposed surrogate method against the state-of-the-art DL-based methods in accurately forecasting the EV charging demand and EV flows in the TUE, while coping with the multi-dimensional uncertainties of the TAP, as well as its computational superiority. Qualitative results also revealed

the beneficial impact of the proposed coordinated optimization of EV flows and charging demand on the operation of both TN and PDN.

Future work aims at enhancing the proposed ECCN-DBN method in two directions. The first one lies in applying discharging facility during the charging process to consider the diversity of charging demand and the associate operational cost of PDN. The second one lies in making the multi-period charging/discharging decisions using the proposed surrogate model to minimize the cost of EV users as well as the total cost of TN and PDN systems, going beyond the settings examined in this paper, where the charging period of each EV is fixed.

References

[1] M. Isik, R. Dodder, P. O. Kaplan, Transportation emissions scenarios for New York City under different carbon intensities of electricity and electric vehicle adoption rates, Nat. Energy 6 (Jan. 2021) 92–104.

[2] H. Das, M. Rahman, S. Li, C. Tan, Electric vehicles standards, charging infrastructure, and impact on grid integration: A technological review, Renew. Sustain. Energy Rev. 120 (Mar. 2020) 109618.

[3] International Energy Agency, Global EV outlook 2021, prospects for electric vehicle deployment, https://www.iea.org/reports/global-ev-outlook-2021, 2021.

[4] H. Kikusato, K. Mori, S. Yoshizawa, Y. Fujimoto, H. Asano, Y. Hayashi, A. Kawashima, S. Inagaki, T. Suzuki, Electric vehicle charge–discharge management for utilization of photovoltaic by coordination between home and grid energy management systems, IEEE Trans. Smart Grid 10 (May 2019) 3186–3197.

[5] H. Patil, V. N. Kalkhambkar, Grid integration of electric vehicles for economic benefits: A review, J. Mod. Power Syst. Clean Energy 9 (Jan. 2021) 13–26.

[6] H. Zhang, S. J. Moura, Z. Hu, Y. Song, PEV fast-charging station siting and sizing on coupled transportation and power networks, IEEE Trans. Smart Grid 9 (2018) 2595–2605.

[7] Y. Sun, Z. Chen, Z. Li, W. Tian, M. Shahidehpour, EV charging schedule in coupled constrained networks of transportation and power system, IEEE Trans. Smart Grid 10 (Sep. 2019) 4706–4716.

[8] G. Zhang, S. T. Tan, G. G. Wang, Real-time smart charging of electric vehicles for demand charge reduction at non-residential sites, IEEE Trans. Smart Grid 9 (2018) 4027–4037.

[9] Q. Yan, B. Zhang, M. Kezunovic, Optimized operational cost reduction for an EV charging station integrated with battery energy storage and PV generation, IEEE Trans. Smart Grid 10 (2019) 2096–2106.

[10] Y. Zhang, J. Chen, L. Cai, J. Pan, Expanding EV charging networks considering transportation pattern and power supply limit, IEEE Trans. Smart Grid 10 (2019) 6332–6342.

[11] Q. Yuan, Y. Tang, Electric vehicle demand response technology based on traffic-grid coupling networks, Proc. CSEE 41 (Mar. 2020) 1627–1636.

[12] M. van Essen, O. Eikenbroek, T. Thomas, E. van Berkum, Travelers' compliance with social routing advice: Impacts on road network performance and equity, IEEE Trans. Intell. Transp. Syst. 21 (2020) 1180–1190.

[13] G. Ferro, R. Minciardi, M. Robba, A user equilibrium model for electric vehicles: Joint traffic and energy demand assignment, Energy 198 (May 2020) 117299.

[14] T. Qian, C. Shao, X. Li, X. Wang, M. Shahidehpour, Enhanced coordinated operations of electric power and transportation networks via EV charging services, IEEE Trans. Smart Grid 11 (2020) 3019–3030.

[15] W. Wei, S. Mei, L. Wu, M. Shahidehpour, Y. Fang, Optimal traffic-power flow in urban electrified transportation networks, IEEE Trans. Smart Grid 8 (2017) 84–95.

[16] W. Wei, L. Wu, J. Wang, S. Mei, Network equilibrium of coupled transportation and power distribution systems, IEEE Trans. Smart Grid 9 (2018) 6764–6779.

[17] W. Jing, I. Kim, M. Ramezani, Z. Liu, Stochastic traffic assignment of mixed electric vehicle and gasoline vehicle flow with path distance constraints, Transp. Res. Proc. 21 (2017) 65–78.

[18] H. Ye, On stochastic-user-equilibrium-based day-to-day dynamics, Transp. Sci. (2021).

[19] A. J. Pel, E. Chaniotakis, Stochastic user equilibrium traffic assignment with equilibrated parking search routes, Transp. Res. B Meth. 101 (2017) 123–139.

[20] D. P. Watling, T. K. Rasmussen, C. G. Prato, O. A. Nielsen, Stochastic user equilibrium with a bounded choice model, Transp. Res. B Meth. 114 (2018) 254–280.

[21] Y. Ye, D. Qiu, X. Wu, G. Strbac, J. Ward, Model-free real-time autonomous control for a residential multi-energy system using deep reinforcement learning, IEEE Trans. Smart Grid 11 (2020) 3068–3082.

[22] J. Zhao, F. F. Li, X. Chen, Q. Wu, Deep learning based model-free robust load restoration to enhance bulk system resilience with wind power penetration, IEEE Trans. Power Syst. (2021).

[23] X. Wang, Y. Liu, J. Zhao, C. Liu, J. Liu, J. Yan, Surrogate model enabled deep reinforcement learning for hybrid energy community operation, Appl. Energy 289 (2021) 116722.

[24] N. Yang, J. Jia, C. Xing, S. Liu, D. Chen, D. Ye, Y. Deng, Data-driven intelligent decision-making method for unit commitment based on E-Seq2Seq technology, Proc. CSEE 40 (2020) 7587–7599.

[25] D. Cao, J. Zhao, W. Hu, F. Ding, N. Yu, Q. Huang, Z. Chen, Model-free voltage control of active distribution system with pvs using surrogate model-based deep reinforcement learning, Appl. Energy 306 (Jan. 2022) 117982.

[26] B. Golparvar, P. Papadopoulos, A. A. Ezzat, R.-Q. Wang, A surrogate-model-based approach for estimating the first and second-order moments of offshore wind power, Appl. Energy 299 (Oct. 2021) 117286.

[27] M. Farhoumandi, Q. Zhou, M. Shahidehpour, A review of machine learning applications in IoT-integrated modern power systems, Electr. J. 34 (2021) 106879.

[28] Z. Cui, K. Henrickson, R. Ke, Y. Wang, Traffic graph convolutional recurrent neural network: A deep learning framework for network-scale traffic learning and forecasting, IEEE Trans. Intell. Transp. Syst. 21 (Nov. 2020) 4883–4894.

[29] D. Erhan, P. A. Manzagol, Y. Bengio, S. Bengio, P. Vincent, The difficulty of training deep architectures and the effect of unsupervised pre-training, in: Proc. 12th Intl. Conf. Artif. Intell. Stat. (AISTATS), volume 5, Florida, USA, 2009, pp. 153–160.

[30] G. E. Hinton, S. Osindero, Y. W. Teh, A fast learning algorithm for deep belief nets, Neural Compu. 18 (2006) 1527–1554.

[31] H. L. Li, H. C. Lu, C. H. Huang, N. Z. Hu, A superior representation method for piecewise linear functions, Informs J Comput. 21 (Aug. 2010) 314–321.

[32] J. P. Vielma, Mixed integer linear programming formulation techniques, SIAM Rev. 57 (Feb. 2015) 3–57.

[33] X. Li, J. Li, X. Hu, J. Yang, Line-CNN: End-to-end traffic line detection with line proposal unit, IEEE Trans. Intell. Transp. Syst. 21 (Jan. 2020) 248–258.

[34] J. An, L. Fu, M. Hu, W. Chen, J. Zhan, A novel fuzzy-based convolutional neural network method to traffic flow prediction with uncertain traffic accident information, IEEE Access 7 (Feb. 2019) 20708–20722.

[35] M. Simonovsky, N. Komodakis, Dynamic edge-conditioned filters in convolutional neural networks on graphs, in: Proc. IEEE Conf. Comput. Vis. Pattern Recognit. (CVPR), Honolulu, HI, USA, Jul. 2017, pp. 29–38.

[36] X. Kong, C. Li, F. Zheng, C. Wang, Improved deep belief network for short-term load forecasting considering demand-side management, IEEE Trans. Power Syst. 35 (Mar. 2020) 1531–1538.

[37] H. Z. Wang, G. B. Wang, G. Q. Li, J. C. Peng, Y. T. Liu, Deep belief network based deterministic and probabilistic wind speed forecasting

approach, Appl. Energy 182 (2016) 80–93.

[38] H. Zang, L. Cheng, T. Ding, K. W. Cheung, M. Wang, Z. Wei, G. Sun, Application of functional deep belief network for estimating daily global solar radiation: A case study in china, Energy 191 (2020) 116502.1–116502.16.

[39] G. Hinton, A practical guide to training restricted boltzmann machines, Momentum 9 (Jan. 2010) 926–947.

[40] M. Yan, M. Shahidehpour, A. Alabdulwahab, A. Abusorrah, N. Gurung, H. Zheng, O. Ogunnubi, A. Vukojevic, E. A. Paaso, Blockchain for transacting energy and carbon allowance in networked microgrids, IEEE Trans. Smart Grid 12 (2021) 4702–4714.

[41] V. Freschi, E. Lattanzi, A prim–dijkstra algorithm for multihop calibration of networked embedded systems, IEEE Internet Things J. 8 (Jul. 2021) 11320–11328.

[42] Q. Yuan, Datasheet for PDN implementation related parameters, Nov. 2021. URL: https://dx.doi.org/10.21227/rz33-fp85. doi:10.21227/rz33-fp85.